Stability and energetics of Bursian diodes

M. S. Rosin* and H. Sun
Department of Mathematics, UCLA, Los Angeles, California 90095, USA
(Received 3 December 2012; published 26 April 2013)

We present an analysis of the stability, energy, and torque properties of a model Bursian diode in a one dimensional Eulerian framework using the cold Euler-Poisson fluid equations. In regions of parameter space where there are two sets of equilibrium solutions for the same boundary conditions, one solution is found to be stable and the other unstable to linear perturbations. Following the linearly unstable solutions into the nonlinear regime, we find they relax to the stable equilibrium. A description of this process in terms of kinetic, potential and boundary-flux energies is given, and the relation to a Hamiltonian formulation is commented on. A nonlocal torque integral theorem relating the prescribed boundary data to the average current in the domain is also provided. The results will be useful for numerical verification purposes, and understanding Bursian diodes in general.

DOI: 10.1103/PhysRevE.87.043114 PACS number(s): 52.75.Fk, 47.10.ab, 85.45.Db, 52.25.Fi

I. INTRODUCTION

In its simplest form, a diode consists of two conducting electrodes with a relative electric potential bias $|\phi_1|$ and a distribution of moving charge carriers. Fundamentally, the transport of these charge carriers is constrained, self-consistently, by nonlinear space charge effects. For example, in the case of a steady un-neutralized electron flow in one dimension (a Bursian diode), the charge flux cannot exceed the analytically derivable Child-Langmuir limit that depends only on $|\phi_1|$, the size of the domain and the velocity of the incoming electrons [1–3]. Mechanistically, if the electron flux exceeds the limiting value, there is a charge build-up—a virtual cathode—and an associated electric field that resists the passage of additional electrons.

Understanding and controlling the onset of this virtual cathode, as well as other, nearby, physically and numerically accessible states, their stability properties, and the energy demands of maintaining a diode flow, has applications in a wide range of settings that are well reviewed by Ender *et al*. [4]. Some examples include inertial-electrostatic confinement [5], pinch reflex diodes for intense ion beam generation [6], vircators [7], reflex triodes for microwave generation [8], photoinjectors [9,10], and producing GHz to THz electromagnetic radiation [11,12].

Historically, much of the illuminating analysis has come from simulations, especially in complex geometries and for kinetic systems. To ensure the fidelity of future codes, a good understanding of the basic physics and a suite of test cases for benchmarking is desirable. These are an integral part of the verification process [13,14]. Indeed, for just this purpose, there has recently been an explicit call for analytic and high-accuracy numerical solutions for model problems in plasma physics [15–17]. Solutions that meet these requirements would also be of benefit in a wide range of simulation-assisted fields where the equations governing diode dynamics are also applicable: collisional electrostatics, inviscid fluid dynamics, and gravitating astrophysical systems.

On a more primitive level, beyond the industrial applications that can be inferred from simulation, diodes exhibit important fundamental physics. The entering and exiting particles carry with them kinetic and potential energy, thereby making them a readily analyzable, energetically open system. This means that the continuum Hamiltonian description, designed for energetically closed systems, must be extended if it is to be applicable [18,19]. Again, because of the wide applicability of the diode equations to other areas of physics, extending the Hamiltonian formalism would be of significant general importance. A good precursor to any such attempt would be a diode energetics analysis that focused on the role of boundary terms.

To these ends, providing benchmarks for numerical codes and a boundary-inclusive energetics analysis, this paper investigates the linear and nonlinear dynamics of the simple Bursian diode above. In particular, we consider the time-dependent solutions and energy evolution of the two-equilibria region of parameter space.

While this is an old problem with many existing descriptions, e.g., Refs. [3,20], our approach has several original contributions. First, our results are presented in a Eulerian, as opposed to Lagrangian, framework, which is the most generally convenient representation against which to compare numerical simulation. Second, we consider in detail the *intermediate* nonlinear regime of solutions that exists beyond the linear stage and before the final relaxed state is reached. It is in this regime, where the nonlinear dynamics compete with the electrostatically driven relaxation, that code irregularities will most likely appear. While the initial and final states of a perturbed Bursian diode in the two-equilibria region are well know, *how* the system transitions between these states is not. Finally, we present new interpretations and parallels between disperate areas of physics that have not been previously discussed: diodes, the role of torque conservation, and, briefly, astrophysics.

The plan of this paper is as follows. In Sec. II we introduce our equations and review what is known about their time-independent, i.e., equilibrium, solutions. We focus on regions of parameter space that support two distinct equilibria. In Sec. III we present a new perspective on their linear stability, showing one to be stable and the other unstable. In Sec. IV we

*Mailing address: Lawrence Livermore National Lab and L-637, P. O. Box 808, Livermore, CA 94511-0808; msr35@math.ucla.edu

 ©2013 American Physical Society

continue our investigation by following the linear instability into the nonlinear regime and discuss the associated system energy and torque and their role as diagnostics. In Sec. V we conclude and discuss some potential applications for our results.

II. EQUILIBRIUM SOLUTIONS

The physical picture of a working Bursian diode is one of electrons flowing across a diode domain under the influence of an electric potential. The potential is made up of an external component that is determined by the boundary conditions at the incoming and outgoing edges, and an internal potential that is determined self-consistently by Poisson's equation.

When the electrons are cold and collisionally dominated, this systems is described by the Euler-Poisson fluid equations

$$\partial_t \rho + \partial_x(\rho v) = 0, \tag{1}$$

$$\partial_t v + v\partial_x v = \partial_x \phi, \tag{2}$$

$$\partial_{xx}\phi = \rho. \tag{3}$$

Here x, t, ρ, v, and ϕ are the scaled position, time, density, velocity, and potential for an electron fluid. The hyperbolic equations (1) and (2), respectively, describe the conservation of mass, and the momentum evolution of a fluid element forced by an electric field $-\partial_x\phi$. Equation (3) relates the electric potential to the charge density via the elliptic Poisson equation.

To determine the external electric potential, and incoming electron density and velocity, we introduce the following time-independent Dirichlet boundary conditions:

$$\left.\begin{array}{l}\phi = 0\\ v = v_0\\ \rho = \rho_0\end{array}\right\} \quad \text{on} \quad x = 0$$

$$\phi = \phi_1 \qquad \text{on} \quad x = d. \tag{4}$$

Here $x = 0$ is the incoming boundary and $x = d$ is the outgoing boundary, so electrons flow from 0 to d. Equations (1)–(4) have been normalized using

$$(x,t,v,\phi,\rho) = (x'/L, t'/T, v'/(L/T), \phi'/\varphi, \rho'/R)$$
$$\varphi = (m_e/q_e)(L/T)^2 \quad R = (\varepsilon_0/q_e)(\varphi/L^2),$$

where the primed variables are unscaled, L and T are characteristic length and time scales, m_e is the electron mass, q_e the fundamental charge (positive), and ε_0 is vacuum permittivity.

In the steady state (1) and (2) constrain the current ρv and the energy density of a fluid element, kinetic plus potential $v^2/2 - \phi$, to be constant across the domain (the minus is because electrons are negatively charged). This implies that for given boundary conditions, i.e., (4), the two unspecified fields at the outgoing boundary $\rho(d), v(d)$ are uniquely determined. The motion of the fluid can be understood energetically in terms of Hamilton's principle, the principle of least action, from which (2) can be derived. The gain (loss) in the kinetic energy of a fluid element as it crosses the domain equals its loss (gain) in potential energy as work is done on (against) it by the electric field (that accelerates electrons from the emitting cathode to the collecting anode, in the case of a monotonically increasing potential).

It is known that there are two kinds of equilibrium solutions to the system (1)–(4), and we review them here [3]. For $\phi_1 > 0$, their implicit expressions are given by

$$(\Phi - 2\alpha)\sqrt{\Phi + \alpha} = \frac{3}{4}\frac{\sqrt{8\rho_0}}{v_0}x + (1 - 2\alpha)\sqrt{1 + \alpha}, \tag{5}$$

$$(\Phi - 2\alpha)\sqrt{\Phi + \alpha} = \left|\frac{3}{4}\frac{\sqrt{8\rho_0}}{v_0}x - (1 - 2\alpha)\sqrt{1 + \alpha}\right|, \tag{6}$$

where $\Phi = \sqrt{1 + 2\phi/v_0^2}$ and $\Phi_d = \sqrt{1 + 2\phi_1/v_0^2}$ are normalized potentials. The quantities $\xi_1 = 4/3(1 + \Phi_d^{3/2}) < \xi_2 = 4/3(\Phi_d + 2)(\Phi_d - 1)^{1/2} < \xi_3 = 4/3(1 + \Phi_d)^{3/2}$ demarcate (nonexclusively) the boundaries between solutions monotonic in ϕ given by (5) that occur when $0 < d\sqrt{8\rho_0/v_0^2} \leqslant \xi_2$, and solutions with a single turning point given by (6) that occur when $\xi_1 < d\sqrt{8\rho_0/v_0^2} \leqslant \xi_3$. The physically relevant difference between (5) and (6) is that, for the former, the electric field always points in one direction and, for the latter, it changes direction. At the reversal point for solutions given by (6), the electric field vanishes and the electrons flow ballistically.

To close (5) and (6) so the functional form of the fields can be determined, α is needed. It satisfies

$$(\Phi_d - 2\alpha)\sqrt{\Phi_d + \alpha} = \frac{3}{4}\frac{\sqrt{8\rho_0}}{v_0}d \pm (1 - 2\alpha)\sqrt{1 + \alpha}, \tag{7}$$

where the positive and negative signs correspond to (5) and (6), respectively.

Necessary and sufficient conditions for determining the number of solutions, zero, one, or two, are given succinctly by

$$d\sqrt{8\rho_0/v_0^2} > \xi_3: \quad \text{zero solutions}, \tag{8}$$

$$d\sqrt{8\rho_0/v_0^2} < \xi_1, \quad \text{or} \quad = \xi_3: \quad \text{one solution}, \tag{9}$$

$$\xi_1 \leqslant d\sqrt{8\rho_0/v_0^2} < \xi_3: \quad \text{two solutions}. \tag{10}$$

The number of accessible solutions is a function of d, v_0, ρ_0, and ϕ_1 (Figs. 1 and 3). For example, for $(d, v_0, \phi_1) = (1, 1, 0.25)$, there are no steady-state solution for $\rho_0 > 2.5$, two when $2.5 > \rho_0 > 1.2$, and one when $\rho_0 < 1.2$. It is important to know these boundaries *a priori* for both modeling and physical testing purposes because of the extreme sensitivity of system around the bifurcation points where the number of solutions changes.

We denote the solution with larger ϕ as branch I and the other as branch II. In the literature, these are known as the C-branch and C-overlap branch, respectively [21].

It is the stability, dynamics, and energy of perturbations to the equilibria in the region of parameter space given by (10) that are the focus of this paper. While these have been investigated before in a Lagrangian framework, our approach in a Eulerian framework is new and has several advantages. Specifically, it allows for a direct interpretation of solutions that are functions of x and t rather than Lagrangian coordinates; the discrete nature of the linear eigenmodes are a natural product of the formulation; and the description is robust to changes that would not allow for a Lagrangian analysis. These features are all useful for verification purposes, as are the expressions (5)–(10) for the equilibrium configuration.

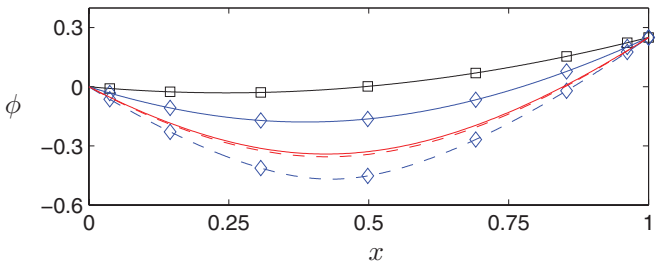

FIG. 1. (Color online) Potential profiles ϕ associated with branch I (solid lines) and branch II (dashed lines) equilibria for $(d,v_0,\phi_0,\phi_1) = (1.0,1.0,0,0.25)$ and $\rho_0 = 2.45$ (red, no symbols), $\rho_0 = 2.00$ (blue, diamonds), and $\rho_0 = 1.00$ (black, squares), respectively. Note that for $\rho = 1.00$ there is only one solution, as given by (9).

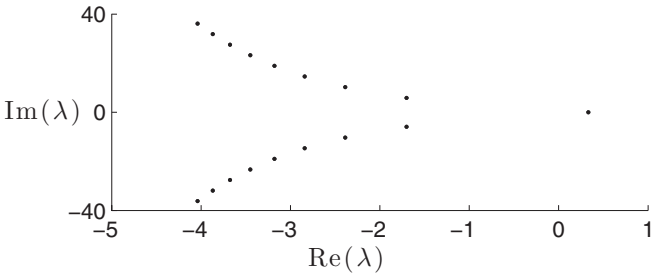

FIG. 2. Eigenvalues associated with perturbations to branch II equilibria with parameters $(d,\rho_0,v_0,\phi_1) = (1,2.4,1,0.25)$. Calculated using Chebyshev spectral methods, only a single positive eigenvalue, the first one, exists, corresponding to an unstable, purely growing mode. The remaining eigenvalues are in complex conjugate pairs with $\mathrm{Re}(\lambda) < 0$, corresponding to damped, traveling waves.

In accordance with earlier studies, we find that the C-overlap branch is unstable to linear perturbations, and we follow these into the nonlinear regime [3,20,22].

III. LINEAR STABILITY ANALYSIS

To provide a set of numerical benchmarks for verification purposes, and to understand the physics of Bursian diodes at small times, we conduct a perturbation analysis. We wish to determine the linear stability properties of branch I and branch II equilibrium solutions to (1)–(3) when (10) holds. To do so, we use (5)–(7) subject to (4) to construct equilibria $\tilde{\rho}(x)$, $\tilde{v}(x)$, $\tilde{\phi}(x)$, and to these we add small perturbations $(\delta\rho,\delta v,\delta\phi) = (\delta\rho(x),\delta v(x),\delta\phi(x))e^{\lambda t}$ that obey $(\delta\rho,\delta v,\delta\phi) = (0,0,0)$ at $x = 0$ and $\delta\phi = 0$ at $x = d$.

Linearizing, we obtain

$$\lambda\delta\rho + \partial_x(\tilde{\rho}\delta v) + \partial_x(\tilde{v}\delta\rho) = 0, \tag{11}$$

$$\lambda\delta v + \partial_x(\tilde{v}\delta v) = \partial_x\delta\phi, \tag{12}$$

$$\partial_{xx}\delta\phi = \delta\rho. \tag{13}$$

This system can be written as

$$\lambda\begin{pmatrix}\delta\rho\\ \delta v\end{pmatrix} = A\begin{pmatrix}\delta\rho\\ \delta v\end{pmatrix}, \tag{14}$$

where

$$A := \begin{bmatrix}-\partial_x\tilde{v} - \tilde{v}\partial_x & -\partial_x\tilde{\rho} - \tilde{\rho}\partial_x\\ \partial_x(\partial_{xx})^{-1} & -\partial_x\tilde{v} - \tilde{v}\partial_x\end{bmatrix}. \tag{15}$$

The eigenvalues of (14) determine the linear stability of the system as follows: $\mathrm{Re}(\lambda) > 0$ describes unstable modes and $\mathrm{Re}(\lambda) < 0$ describes stable modes. To compute λ, we discretize the operator matrix (15) using three methods: a uniform grid with an upwind scheme, a uniform grid with a centered difference scheme, and a Chebyshev grid with an associated polynomial interpolation [23]. The discrete spectrum of eigenvalue-eigenvector solutions—a discreteness not generally emphasized in the dispersion relations arising from Lagrangian analyses, e.g., Refs. [20,22]—are obtained numerically and shown in Figs. 2, 4, and 5. All three schemes converge to the same consistent result. We take this to constitute a "high-accuracy numerical solution," and below a numerical example is provided for testing purposes.

Conducting a parameter scan, for branch II we find $\lambda > 0 \in \mathrm{Re}$ for the first eigenvalue, the one with a single zero in the corresponding eigenfunctions. For the remaining eigenvalues in branch II, and all of branch I, $\mathrm{Re}(\lambda) < 0$. The system supports a single unstable mode. For example, for $(d,\rho_0,v_0,\phi_1) = (1,1.5,1,0.2)$, the most positive eigenvalues from branch II and I are 1.1 and −2.1 respectively: One mode is unstable and the other stable. As the two equilibrium solutions merge at $d\sqrt{8\rho_0/v_0^2} = \xi_3$, the unstable eigenvalue of branch II obeys $\mathrm{Re}(\lambda) \to 0$. Approaching the other boundary of the two solution region $d\sqrt{8\rho_0/v_0^2} = \xi_1$, the full-width at half-maximum of the corresponding eigenmode $\to 0$. It remains to be seen whether this singular mode bears any fundamental relation to the singularity that forms in the case that the current exceeds the Child-Langmuir limit [24,25].

The physical implications of these results is that for any experimental realization, branch II solutions cannot persist for any extended period. Infinitesimal perturbations arising from any source of broadband background noise will, under an appropriate decomposition, support an unstable mode. This mode will grow at an exponential rate λ, moving the total solution $(\tilde{\rho}(x), \tilde{v}(x), \tilde{\phi}(x)) + (\delta\rho,\delta v,\delta\phi)$ away from its initial branch II configuration. While the inherent instability of branch II solutions are well known [20], the growth rates and fields configurations are not, at least in terms of the boundary conditions and Eulerian formulation, used here.

Furthermore, discussion of the medium term fate of the unstable solutions has been largely neglected in the literature. In the next section we address this by following the perturbations into the nonlinear regime and to their final, stable state.

IV. NONLINEAR DYNAMICS

For small time, coupling between infinitesimal amplitude perturbations, and their feedback on the equilibrium solutions, is negligible. However, because $\lambda > 0$ for one mode, that mode grows exponentially and the perturbations quickly reach nonlinear amplitudes. In this case, the methods and results of Sec. III are no longer applicable. In the nonlinear regime, the most general method for solving (1)–(3) is numerical integration; although the method of characteristics can also be used to obtain complete analytic solutions in a Lagrangian framework [4,22]. The method used here, a Eulerian approach,

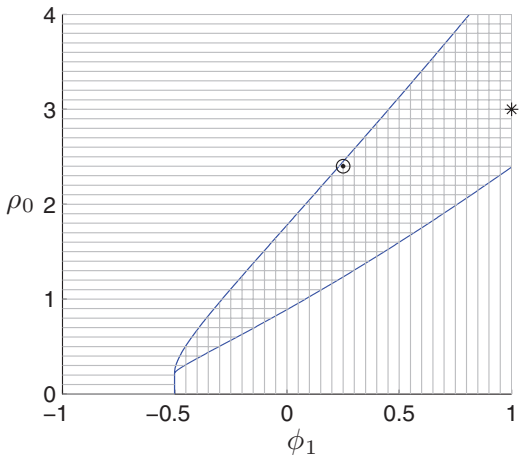

FIG. 3. (Color online) Number of equilibrium solutions to (1)–(3) as follows: Zero (horizontal lines), one (vertical lines), and two (crossing lines) for varying ρ_0,ϕ_1 and $(d,v_0) = (1,1)$. The zero- and two-solution boundary at $d\sqrt{8\rho_0/v_0^2} = \xi_3$ corresponds to the space charge limiting current derived by Child and Langmuir for $v_0 = 0$, Jaffé for $v_0 > 0$, and Caflisch and Rosin for time-varying boundary conditions [1–3,24]. The circled dot corresponds to the parameters used in Fig. 2 and the star to those in Figs. 5, 6, and 7.

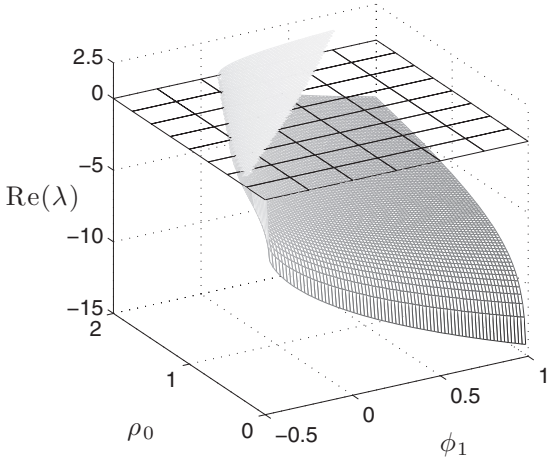

FIG. 4. The most positive eigenvalues of (14), i.e., λ, associated with perturbations to branch II [Re(λ) > 0, unstable] and branch I [Re(λ) < 0, stable] solutions for the parameters $(d,v_0) = (1,1)$, and varied ρ_0 and ϕ_1; see Fig. 3.

has the advantage that it is naturally formulated as a two-point Dirichlet boundary value problem for ϕ, which can easily be realized experimentally, i.e., ϕ is prescribed on both boundaries. The alternative Lagrangian approach is more naturally formulated as a Cauchy problem, which is harder to realize experimentally and from which the corresponding Dirichlet conditions are nontrivial to obtain [24], i.e., ϕ and $\partial_x\phi$ are prescribed on one boundary. In terms of the relative verification merits of the methods, it is worth noting that a Lagrangian analysis must be numerical remapped before it can be compared to the solution produced by a Eulerian code.

We favor the direct Eulerian numerical approach. We employ MacCormack's method to integrate the hyperbolic equations (1)–(2) and solve the elliptic Poisson equation (3) at each time step using a finite-difference description and inverting a tridiagonal matrix. Our simulations are initialized with unstable equilibrium solutions from branch II and numerical noise provides broadband perturbations which are constrained to obey (4). The solutions to our perturbed system are well matched by our linear results for small time, and in the final state the solutions have relaxed to the stable branch I equilibrium solutions with the same boundary conditions as the initial, unstable equilibrium (Fig. 6).

Physical insight and a set of numerical benchmarks for the system can be obtained by considering both the energetics of the system and its global torque. In the next subsection, we examine each in turn and derive a set of integral equations that describe the system's spatially averaged properties and their interaction with the boundaries.

These types of equations are both less computationally demanding to solve (which is unimportant here but may matter in higher dimensions or kinetic models) and do not require knowledge of the fundamental unaveraged solutions. Furthermore, being able to relate *prescribed* boundary value data to *derived* domain data offers a new avenue for both control and experimental measurement of spatially distributed system properties.

A. Energetics

Even at the model equation level considered here, energy insights may be important for industrial purposes [7]. In this subsection, we examine the evolution and balance of the standard energy integrals. We leave further detailed discussion to a forthcoming paper in which we present a tailored Bursian diode-battery model.

We start by multiplying (2) by v and combining it with (1) to yield an evolution equation for the kinetic energy $\mathcal{K} = \rho v^2/2$ balance of the system,

$$\partial_t \mathcal{K} + \partial_x (v\mathcal{K}) = \rho v \partial_x \phi, \tag{16}$$

where $\rho v\partial_x\phi$ is the negative Joule heating term. Integrating over x, the total kinetic energy in the system is given by

$$\partial_t \overline{\mathcal{K}} = v_0\mathcal{K}_0 - v_d\mathcal{K}_d + \overline{\rho v \partial_x \phi}, \tag{17}$$

where overbars denotes spatially integrated quantities $\int_0^d dx$ and subscripts $0, d$ indicate that the associated quantity is to be evaluated at $x = 0, d$ respectively. There are two contributions to the total kinetic energy: the difference in the boundary fluxes of kinetic energy and the work done on the fluid by the electric field.

To describe the total energy balance in the system, it helps to decompose $\phi = \phi_E + \phi_I$ into external and internal components, and these satisfy Laplace's and Poisson's equations respectively:

$$\partial_{xx}\phi_E = 0, \quad \text{with} \quad \phi_E(0) = 0, \quad \phi_E(d) = \phi_1, \tag{18}$$

$$\partial_{xx}\phi_I = \rho, \quad \text{with} \quad \phi_I(0) = 0, \quad \phi_I(d) = 0. \tag{19}$$

The solution to (18) is simply $\phi_E = (\phi_1/d)x$, and the Green's function for ϕ_I is

$$\phi_I(x) = \frac{1}{2}\int_0^d dx'\rho(x')\left(|x-x'| - 2\frac{xx'}{d} - x - x'\right). \tag{20}$$

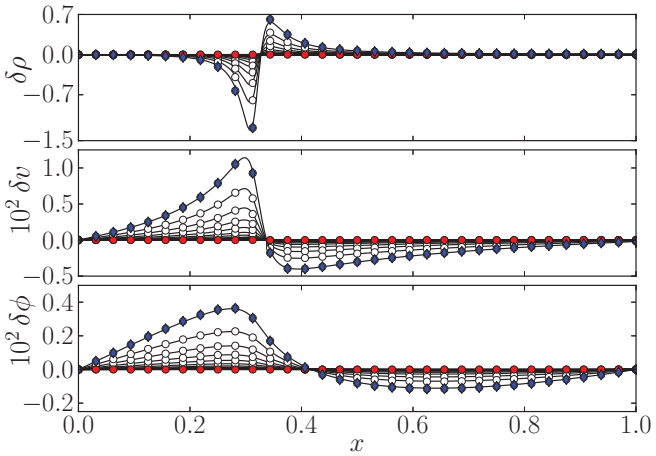

FIG. 5. (Color online) Evolution of perturbed field quantities associated with the unstable branch II equilibrium for $t \leqslant 5.6$ and steady boundary conditions $(d,\rho_0,v_0,\phi_1) = (1,3,1,1)$. Snapshots are every $t = 0.35$ starting from the $\delta\rho,\delta v,\delta\phi = 0$ initial conditions (red circles). The unstable linear eigenmodes (white circles) with growth rate $\exp(\lambda t)$ (Sec. III) overlay the fully nonlinear solutions (solid lines) to $t = 5.5$ (blue diamonds), at which point they start to diverge.

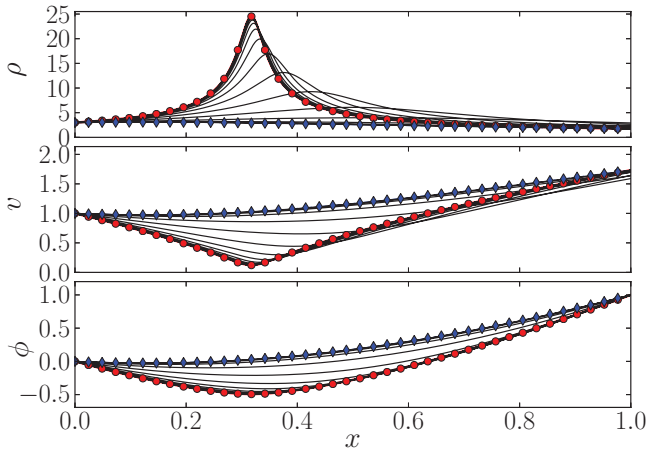

FIG. 6. (Color online) Evolution of full solutions to (1)–(3) starting at the same branch II equilibrium as in Fig. 5, for $t \leqslant 11.5$. Snapshots are every $t = 0.5$, and the initial state (red circles) is given by (5)–(7). The final state (blue diamonds) is the same stable branch I equilibrium derived from the same set of equations and boundary conditions as the initial state.

Rewriting (16) in conservative form using (1) and (19), we have

$$\partial_t \mathcal{E} + \partial_x \left[v \left(\mathcal{E} + \mathcal{P}_\mathrm{I} \right) \right] = 0, \tag{21}$$

where $\mathcal{E} = \mathcal{K} + \mathcal{P}_\mathrm{E} + \mathcal{P}_\mathrm{I}$ is the combined kinetic $\mathcal{K}$, external potential $\mathcal{P}_\mathrm{E} = -\rho\phi_\mathrm{E}$ and internal potential $\mathcal{P}_\mathrm{I} = -\rho\phi_\mathrm{I}/2$ energy of a fluid element, and we have made use of the fact that $\phi_\mathrm{E}, \phi_\mathrm{I}(0)$, and $\phi_\mathrm{I}(d)$ are time independent. Physically, the factor of a half in the definition of $\mathcal{P}_\mathrm{I}$ is to avoid double counting particle interaction energies [26]. Mathematically, it arises from the symmetry properties of the Green's function (20) under $x \Leftrightarrow x'$.

In the absence of net boundary fluxes, the second term in (21) vanishes on integration. In this case, the total energy $\overline{\mathcal{E}}$ is conserved and coincides with the fluid Hamiltonian $\mathcal{H} = \rho v^2/2 + (\partial_x\phi)^2/2$, from which the equation of motion (2) can be derived [11,27]. The evolution of the various energy quantities is plotted in Fig. 7.

Considerable work has been done on the nonlinear stability of closed plasma and fluid systems using variational principles, e.g., Refs. [28–31]. However, for open systems, i.e., ones with sources, like boundary fluxes, stability proofs are difficult to construct, and we do not attempt to do so here. Nevertheless, the nonlinear stability and Hamiltonian structure of such systems has been the focus of recent work, and so a theorem tailored to the problem described here may be forthcoming [32–35].

B. Torque and boundary conditions

Unlike energy, torque is not generally considered as an important property of diode systems. However, it is frequently invoked in describing stellar systems governed by (1)–(3), in the context of which (2) is known as the Jeans equation and ϕ is the gravitational potential. We consider it here too and derive a simplified lower moment analog to the astrophysical virial theorem, including boundary effects [36]. As for the virial theorem, we find a "basic structural relation that the system must obey" [37].

To proceed, we note that, uniquely, the 1D version of Poisson's equation (3) can be directly integrated to yield

$$\int_0^x dx\,\partial_{xx}\phi = \partial_x\phi(x) - \partial_x\phi(0) = \int_0^x dx'\rho(x'), \tag{22}$$

where the right-hand side is the mass between 0 and x which can vary with time, and we now denote as $M(x) := M_x$. It follows from (22) that

$$\begin{aligned}\phi_1 &= \int_0^d dx \left[\int_0^x dx'\rho(x') + \partial_x\phi(0) \right] \\ &= M_d\,(d - \overline{x}) + \partial_x\phi(0)d,\end{aligned} \tag{23}$$

where $\overline{x} \equiv \int_0^d dx\,x\rho / \int_0^d dx\rho$ is, by definition, the center of mass.

Equation (23) has a very simple interpretation. By definition, the torque about a point d is $T = Fr$, where r is the magnitude of the directional vector joining d and the point at which F, the force perpendicular to this vector, acts. Let us consider a force acting at the system's center of mass $\overline{x}$, proportional to the total mass M_d, and perpendicular to ∇x, say, a gravitational force $F = M_d g$. In this case, we have $T = M_d g(d - \overline{x})$, and so

$$\phi_1 - \partial_x\phi(0)d = (d - \overline{x})M_d \equiv T, \tag{24}$$

where we have absorbed g into the definition of T. For time-independent $\phi_1 - \partial_x\phi(0)d$, this implies that the total torque on the system is constant.

This results in an interesting relation between the current, the rate of change of the incoming electric field $\partial_t\partial_x\phi(0)$, and the exiting potential $\partial_t\phi_1$. Differentiating (24),

$$\partial_t T = -\partial_t\overline{x}M_d + (d - \overline{x})\partial_t M_d = \partial_t[\phi_1 - \partial_x\phi(0)d], \tag{25}$$

and, using (1), we have

$$\partial_t M_d = -\int_0^d dx\,\partial_x(\rho u) = \rho_0 u_0 - \rho_d u_d, \tag{26}$$

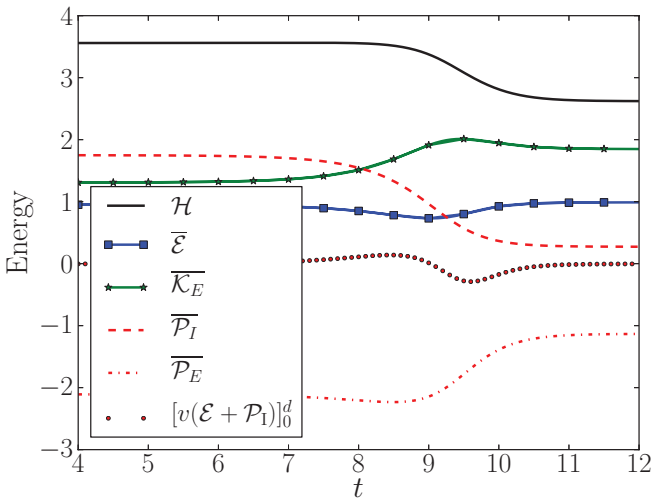

FIG. 7. (Color online) Evolution of the total (spatially integrated) energy of a Bursian diode system from an initial unstable equilibrium solution (branch II) to a final stable equilibrium solution (branch I) for the same set of boundary conditions as in Fig. 5. While the final total energy state $\overline{\mathcal{E}}$ is slightly greater than the initial state, the Hamiltonian $\mathcal{H}$ is a strictly decreasing function of time. The system's dominant form of energy switches to kinetic $\overline{\mathcal{K}}$ from internal potential energy $\overline{\mathcal{P}_I}$ as time progresses, and in the final state the net boundary flux of energy $[v(\mathcal{E}+\mathcal{P}_I]_0^d$ is zero.

$$\partial_t \overline{x} M_d = -d\rho_d u_d + J(d) - \partial_t M_d\, \overline{x}, \tag{27}$$

where $J(d) \equiv \int_0^d dx\, \rho u$ is the current in the domain, and (26) simply states that the rate of change of mass is the flux in minus the flux out.

Combining (25), (26), and (27) we find

$$\rho_0 u_0 = d^{-1}(J(d) + \partial_t \phi_1) - \partial_t \partial_x \phi(0), \tag{28}$$

which is the main result of this subsection [38].

Equation (28) relates the average current in the domain, a derived quantity, to a set of boundary data. This, potentially, affords a new avenue for control. As mentioned earlier, because (1)–(3) can be written in characteristic form, in a mathematical sense, the appearance of the incoming electric field $-\partial_x \phi(0)$ is a more natural choice of boundary condition than ϕ_1.

V. CONCLUSIONS

While Bursian diodes have been well studied over the past century, the advent of large-scale, multidimensional particle-in-cell codes and fluid codes in complex geometries have the potential to offer new insights into their basic physics and to guide their design. The work provided here, while relatively basic, provides a reliable set of analytic and high-accuracy numerical results against which the results of advanced code bases can be *verified* [15–17]. Specifically, we have included examples throughout the text using particular parameters, as well as Figs. 2, 5, 6, and 7 and Eqs. (24) and (28). Where we have employed numerical tools we have cross-checked our results using multiple methods and conducted appropriate convergence studies.

Our results include a linear stability analysis of the unstable branch II equilibrium (C-overlap branch) and nonlinear simulations of its evolution. We have found that its relaxed state is that of the stable branch I equilibrium with the same boundary conditions. We have also provided a quantitative discussion of the role of energy and torque in diagnosing and controlling the system, and, to the best of our knowledge, our interpretation of the latter is new in the literature.

Possible extensions to this work include constructing a nonlinear stability theorem in the spirit of Bernstein *et al.* but including boundary fluxes [28]; using the results herein for benchmarking more complicated systems, including investigating the stability of Child-Langmuir limited solutions; and prescribing optimizing and efficiency enhancing conditions or frameworks for diode operation [24,39].

ACKNOWLEDGMENTS

Special thanks to R. Caflisch for helpful suggestions throughout and LLNL's Visiting Scientist Program for hosting M.S.R. Also thanks to C. Anderson, B. Cohen, A. Dimits, M. Dorf, T. Heinemen, J. Hannay, S. Lee, L. LoDestro, A. Mestel, P. Morrison, L. Ricketson, D. Ryutov, and D. Uminsky for useful conversations. This work was funded by the Department of Energy through Grant No. DE-FG02-05ER25710 (M.S.R.), the Air Force Office of Scientific Research STTR program through Grant No. FA9550-09-C-0115 (H.S.), and NSF Grant No. DMS-0907931 (H.S.).

[1] C. Child, Phys. Rev. (Series I) **32**, 492 (1911).
[2] I. Langmuir, Phys. Rev. **2**, 450 (1913).
[3] G. Jaffé, Phys. Rev. **65**, 91 (1944).
[4] A. Ender, H. Kolinsky, V. Kuznetsov, and H. Schamel, Phys. Rep. **328**, 1 (2000).
[5] M. Carr and J. Khachan, Phys. Plasmas **17**, 052510 (2010).
[6] D. Hinshelwood, P. Ottinger, J. Schumer, R. Allen, J. Apruzese, R. Commisso, G. Cooperstein, S. Jackson, D. Murphy, D. Phipps *et al.*, Phys. Plasmas **18**, 053106 (2011).
[7] D. Sullivan, J. Walsh, and E. Coutsias, *Virtual Cathode Oscillator (vircator) Theory*, Vol. 13 (Artech House, Norwood, MA, 1987).
[8] A. Sharma, S. Kumar, S. Mitra, V. Sharma, A. Patel, A. Roy, R. Menon, K. Nagesh, and D. Chakravarthy, IEEE Trans. Plasma Sci. **39**, 1262 (2011).
[9] E. A. Coutsias and D. J. Sullivan, Phys. Rev. A **27**, 1535 (1983).
[10] Á. Valfells, D. Feldman, M. Virgo, P. O'Shea, and Y. Lau, Phys. Plasmas **9**, 2377 (2002).
[11] P. Akimov, H. Schamel, H. Kolinsky, A. Ender, and V. Kuznetsov, Phys. Plasmas **8**, 3788 (2001).
[12] A. Pedersen, A. Manolescu, and Á. Valfells, Phys. Rev. Lett. **104**, 175002 (2010).
[13] W. L. Oberkampf and T. G. Trucano, Progr. Aerospace Sci. **38**, 209 (2002).

[14] M. Greenwald, Phys. Plasmas **17**, 058101 (2010).
[15] M. M. Turner and M. Vukovic, *Overview of Verification and Validation in Low Temperature Plasma Physics*, Vol. 57 (APS, Washington, DC, 2012).
[16] S. Samukawa, M. Hori, S. Rauf, K. Tachibana, P. Bruggeman, G. Kroesen, J. C. Whitehead, A. B. Murphy, A. F. Gutsol, S. Starikovskaia *et al*., J. Phys. D **45**, 253001 (2012).
[17] Michigan State University, Workshop, *Algorithm and Model Verification and Validation for Kinetic Plasma Simulation Codes* (2012), http://www.egr.msu.edu/amvv2012/home.
[18] R. Salmon, Annu. Rev. Fluid Mech. **20**, 225 (1988).
[19] P. Morrison, Rev. Mod. Phys. **70**, 467 (1998).
[20] R. Lomax, Proc. IEEE Monogr. **108**, 119 (1961).
[21] C. Fay, A. Samuel, and W. Shockley, Bell Syst. Tech. J. **17** (1938).
[22] H. Kolinsky and H. Schamel, J. Plasma Phys. **57**, 403 (1997).
[23] L. N. Trefethen, *Spectral Methods in MATLAB* (SIAM, Philadelphia, PA, 2000).
[24] R. E. Caflisch and M. S. Rosin, Phys. Rev. E **85**, 056408 (2012).
[25] E. Coutsias, J. Plasma Phys. **40**, 369 (1988).
[26] J. Jackson, *Classical Electrodynamics* (John Wiley & Sons, New York, 1965).
[27] D. Holm, Phys. Lett. A **114**, 137 (1986).
[28] I. Bernstein, E. Frieman, M. Kruskal, and R. Kulsrud, Proc. R. Soc. London A **244**, 17 (1958).
[29] D. Holm, J. Marsden, T. Ratiu, and A. Weinstein, Phys. Rep. **123**, 1 (1985).
[30] P. Morrison, Z. Naturforsch **42a**, 1115 (1987).
[31] G. Rein, Arch. Ration. Mech. Anal. **168**, 115 (2003).
[32] A. Van der Schaft and B. Maschke, J. Geom. Phys. **42**, 166 (2002).
[33] D. Jeltsema and A. Schaft, J. Phys. A: Math. Theor. **40**, 11627 (2007).
[34] D. Jeltsema and A. Van Der Schaft, Rep. Math. Phys. **63**, 55 (2009).
[35] G. Nishida and N. Sakamoto, *Hamiltonian Representation of Magnetohydrodynamics for Boundary Energy Controls, Topics in Magnetohydrodynamics* (InTech, New York, 2012), http://www.intechopen.com/books/topics-in-magnetohydrodynamics/hamiltonian-representation-of-magnetohydrodynamics-for-boundary-energy-controls.
[36] S. Chandrasekhar, *The Higher Order Virial Equations and Their Applications to the Equilibrium and the Stability of Rotating Configurations*, Lectures in Theoretical Physics, Vol. 6 (University of Colorado Press, Boulder, 1964).
[37] G. Collins *et al*., *The Virial Theorem in Stellar Astrophysics*, Vol. 1 (Tucson Ariz., Pachart, 1977).
[38] An alternative derivation of this result due to R. Caflisch (private communication) can be obtained by simply evaluating the Green's function solution of (3) for ϕ at $x = d$ with appropriate boundary conditions.
[39] M. Griswold, N. Fisch, and J. Wurtele, Phys. Plasmas **17**, 114503 (2010).